2022 19th International Conference on Electrical Engineering, Computing Science and Automatic Control (CCE). Mexico City, Mexico. November 9-11, 2022.

2D NIR-SPI spatial resolution evaluation under scattering condition.

Carlos Alexander Osorio Quero
Electronics Department.
Instituto Nacional de Astrofísica, Óptica y Electrónica (INAOE)
Puebla, Mexico
caoq@inaoep.mx

Daniel Durini
Electronics Department.
Instituto Nacional de Astrofísica Óptica y Electrónica (INAOE)
Puebla, Mexico
ddurini@inaoep.mx

Jose de Jesus Rangel-Magdaleno
Electronics Department.
Instituto Nacional de Astrofísica Óptica y Electrónica (INAOE)
Puebla, Mexico
jrangel@inaoep.mx

Jose Martinez-Carranza
Computer Science Department
Instituto Nacional de Astrofísica Óptica y Electrónica (INAOE)
Puebla, Mexico
carranza@inaoep.mx

Ruben Ramos-Garcia
Optical Department
Instituto Nacional de Astrofísica Óptica y Electrónica (INAOE)
Puebla, Mexico
rgarcia@inaoep.mx

***Abstract*—In recent years, it had been an evolution in the sensors used by vision systems. Different technologies from RGB camera, IR-camera, LIDAR, RADAR, or sensor combinations can work in different spectrum bands. A new alternative to the vision system is the single-pixel camera (SPC), an architecture based on the compressive sensing theory for 2D reconstruction images. SPC's feature is used as the single detector that measures the linear combinations of pixels through patterns projection of structured light over the object that would like to photograph instead of using an array of pixels as in RGB sensors or cameras. These architectures offer the advantage that they can be adapted to different spectrum bands as near-infrared (NIR), and could operate in scenarios with low visibility or under rain, mist, or fog conditions. Currently, there is little information that discusses the problem of spatial resolution in SPC in scattering conditions for which we defined a methodology to evaluate the spatial resolution SPC's in terms of point spread function (PSF), and we analyzed how it affected the spatial resolution with the distance and under foggy conditions, for an SPC with active illumination at the wavelength at 1550 nm.**

***Index Terms*—Single-pixel camera (SPC), Near-infrared (NIR), Hadamard patterns, OMP-Batch-GPU, Line spread function(LSF), point spread function (PSF), spatial resolution, scattering, fog.**

I. Introduction

The Single-Pixel Camera (SPC) is an architecture based on single-pixel imaging (SPI) principle, that uses a single detector as an alternative to the traditional cameras that capture the scene directly using a sensor array. The SPC is based on compressive sensing theory (CS) [1] and uses a single detector combined with devices such as spatial light modulator (SLM), deformable Mirror Device (DMD), or LEDs array [1] to acquire measurements of the scene, which are linear combinations of the virtual pixels. The image of the scene is reconstructed numerically from measurements captured by the photodetector, applying a compressive sensing algorithm, for example, OMP-Batch-GPU [2]. These methods offer the advantage that far fewer measurements are needed to reconstruct accurately. The SPC architecture has these two essential advantages: i) it provides the means to acquire the image in the compressed form, and ii) it is suitable to perform imaging to different wavelengths from which we can take advantage of a wider part of the electromagnetic spectrum, only adapt the photodetector and SLM devices. For which, we can see some applications in infrared [3], terahertz [4], radiation imaging even for space applications as a low power alternative [5].

The spatial resolution is an imaging quality metric for an optical system, for which four main methods are defined in the state-of-the-art for estimation of spatial resolution and depending on the type of optical system (see Table I): i) Resolution test use to determinate of limiting resolution through of resolution target [6], ii) Interferometer using interferometry with coherent laser source [7], iii) MTF using non-interferometric method [8] , and iv) MTF or SFR by using a slanted edge target [9]. However, as applications progress in SPC, there is little information that discusses the problem of resolution [10] [11], and these focus on laboratory tests, and they do not consider scenarios outdoor or with scattering.

This paper focuses on measuring the spatial resolution parameter for NIR-SPI , which is the capacity of the system to distinguish small details on the imaged targets, different from other SPI architectures [1]; we use an active illumination source of 8 x 8 LEDs array. As methods to estimate the spatial resolution, we use MTF using an edge target to calculate the Point Spread Function (PSF) [12], which defines the

978-1-6654-5508-4/22/$31.00 ©2022 IEEE

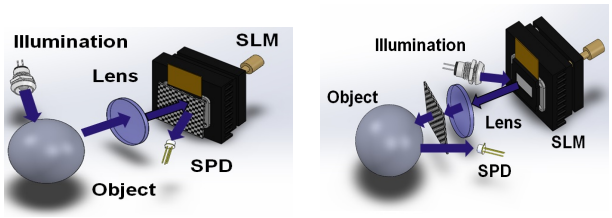

(a) (b)

Fig. 1: Two different approaches applied to SPI: a) Structured detection: the object illuminated by a light source and the light reflected by it gets directed through a lens onto an SLM, where is capture by the SPD, b) Structured illumination: the SLM device project a sequence of patterns and reflected light is capture by the SPD [19].

instrument response to a hypothetical point source [13]. This method is used to evaluate resolution for optical CCD and sensor array cameras [14]; through the use of test charts with complex edge patterns, with that we can be capable of measuring distortions and can be applied to SPCs.

To determine the spatial resolution of our SPC, we will define the PSF calculation experimentally. Therefore, we would start from a method based on circular edge [15], and line spread function (LSF) [16], considering a scattering scenario with fog. The choice of this scenario is due to the fact that the scattering effects are greater in this medium, since the water particles are smaller than the wavelength of the light (Rayleigh scattering [17]). There, we developed a chamber test to simulate the foggy condition to evaluate the spatial resolution in a dispersed medium.

II. SINGLE-PIXEL OBJECT RECONSTRUCTION

The generation of single-pixel images is based on reconstructing the spatial information embedded in the output signals produced by a single-pixel detector (SPD) in response to a sequence of structured illumination patterns created using SLM, DMD, or other similar active illumination technologies. There are two types of configurations that can be used in SPI. Namely, the structured illumination scheme termed front modulation (see Fig. 1a), and a structured detection scheme termed back modulation (see Fig. 1b).

The relationship between the structured and reflected light signal measurement could be expressed using Eq. (1) [20].

$$S_i = \alpha \sum_{x=1}^{M} \sum_{y=1}^{N} O\left(x,y\right) \Phi_i\left(x,y\right) \tag{1}$$

In Eq. (1), (x, y) are the spatial coordinates, O denotes the measured output signal of the used SPD, considering additionally the SPD and the depicted object reflectivities (see Fig. 1) , Φ_i is i_{th} structured pattern of size M x N, S_i is the i_{th} single-pixel measurement corresponding to Φ_i, and α is a constant factor defined by the optoelectronic response of the used SPD. From the previously defined sequence of structured illumination patterns projected onto the scene, and the measured SPD output signals generated in response to each

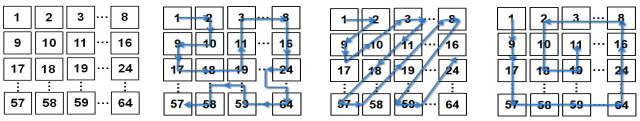

(a) (b) (c) (d)

Fig. 2: Hadamard H_{64} scanning scheme, a) basic Hadamard sequence, b) Hilbert scan [24], c) Zig-Zag scan [22], d) Spiral scan [23].

of those projected illumination patterns, if compressive sensing (CS) algorithms such as OMP-Batch-GPU [2] are applied, the single-pixel image $I(x, y)$ can be reconstructed. The reconstructed image $I(x, y)$ can be defined as the inner product of S_i, the measured output signal generated by the SPD, and the structured illumination pattern $\Phi_i(x, y)$ used to produce the response, additionally proportional to the measured object reflectivity O [20], as expressed in Eq. (2).

$$O\left(x,y\right) = \alpha \sum_{x=1}^{M} \sum_{y=1}^{N} S_i \Phi_i\left(x,y\right) \tag{2}$$

A. Generation of the Hadamard sequence of patterns

The Hadamard pattern [21], defined using Eq. (3), is the most commonly used active illumination pattern in SPI reconstructions, primarily due to its orthogonality properties. To generate a Hadamard matrix, we define it as a square matrix with components defined as +1 or -1, having two distinct rows that coincide in exactly n/2 positions (and therefore disagree in exactly n/2 positions). Furthermore, this matrix H defined must satisfy the condition $HH^T = nI$, where T stands for the transpose of the matrix H, and I represents the identity matrix. Being N, the order of the matrix H,defined in Eq. (3) defines the use of the Kronecker product, where 2^k is an integer with k $>$ 0, and the size of the matrix is defined as M x N.

$$H_{2^k} = \begin{bmatrix} H_{2^{k-1}} & H_{2^{k-1}} \\ H_{2^{k-1}} & -H_{2^{k-1}} \end{bmatrix} = H_2 \otimes H_{2^{k-1}} \tag{3}$$

As an example, Eq. (4) defines a matrix where M = N [21].

$$H_{2^k} = \begin{bmatrix} H\left(1,1\right) & H\left(1,2\right) & ... & H\left(1,N\right) \\ H\left(2,1\right) & H\left(2,2\right) & ... & H\left(2,N\right) \\ ... & ... & ... & ... \\ H\left(M,1\right) & H\left(M,2\right) & ... & H\left(M,N\right) \end{bmatrix} \tag{4}$$

To construct the Hadamard sequence, we used Sylvester's recursive matrix generation principle presented by Eq. (2) [20] to obtain the Hadamard matrix $H_{2^k}(m, n)$. It is important to take into consideration that less than 20 % of m x n Hadamard required limit value decreases the quality of the reconstructed image. One solution to this problem is to apply different types of projection sequences such as "Zig-Zag" [22] (see Fig. 2c), "Spiral" [23] (see Fig. 2d), or "Hilbert trajectory" [24] (see Fig. 2b), where we can defined the sequence of projection in order to achieve a more acceptable trade-off between sampling times and the quality of the final reconstructed images.

TABLE I: Summary of advantages and disadvantages spatial resolution methods [18].

Test method	Vision system	Advantage	Disadvantage
Resolution test	Optical system without sensor Binoculars , and with associated sensors night camera.	Resolution test can be done under simulated field or real day-night condition with high or low target contrast level , and spectral content.	The test is limited to the optical performance of the spectral region ,and it doesn't describe modulation as a function of spatial frequency.
Interferometer	Optical components , optical system without sensors and electronics processing.	MTF measured spatial frequency with high precision.	Limitation on measurement by fewer laser wavelength , and sensitive to ambient vibration. The direct testing of system resolution isn't possible.
MTF	Optical components lenses and without sensors.	Adaptation to perform slanted edge, and MTF measurement by noninterferometric.	Limited of measurement on optical.
MTF or SFR by using a slanted edge target.	Optical system with sensors electronics.	Test focus on digital imaging device with high accuracy, and can be edge target.	Applicable to only digital cameras and another digital imaging device as SPC.

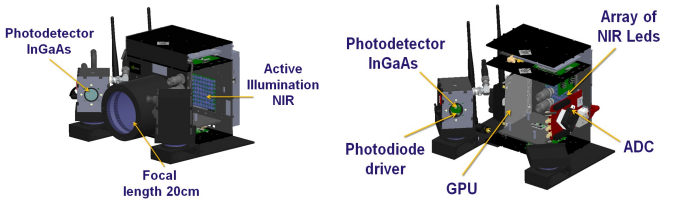

(a) (b)

Fig. 3: Proposed vision system dimension 11 x 12 x 13 cm, focal length 20 cm, weight 1.3 kg, power consumption 25 W, a) first stage module photodiode, active illumination source, photodetector diode InGaAs FGA015,b) second stage GPU unit and ADC [26].

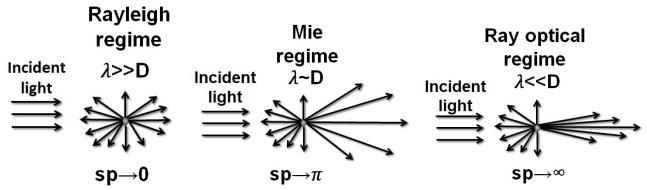

(a) (b) (c)

Fig. 4: Incident beam scattering characteristics for different particles size: a) Rayleigh regime $\lambda >> D$, b) Mie regime $\lambda \sim D$ and c) Ray optical regime $\lambda << D$ [27].

.

B. NIR-SPI camera architecture

In this work, we propose the structured illumination (see Fig. 1b) approach to be applied to a NIR-SPI system based on active illumination provided by an array of 8 x 8 NIR LEDs emitting radiation with a peak wavelength of 1550 nm. An InGaAs photodiode was used as a Single Pixel Detector (SPD). As already explained, this active illumination approach offers several advantages, as it can operate in different outdoor weather conditions under low-level illumination (scenarios with dust, fog, rain, or smoke) and be less sensitive to background radiation noise [25]. The NIR-SPI architecture proposed in this work is divided into two main parts: (i) InGaAs photodetector (diode FGA015 @ 1550 nm), an array of emitting NIR LEDs, and an ADC (see Fig. 3a), and (ii) processing of the electrical signal emitted by the SPD module, digitized using the ADC, and the respective data processing using a Graphics Processing Unit (GPU) (see Fig. 3b). The GPU unit (Jetson Nano) is responsible for generating the Hadamard patterns and processing the converted data by the ADC, used by the OMP-Batch-GPU algorithm [2] running in the GPU unit to generate the 2D images.

III. SCATTERING EFFECT

When light interacts with a water particle in the air, various physical phenomena occur as reflection, refraction, absorption, and scattering. The scattering is related to the particle size (sp), defined as: $sp = \pi D/\lambda$ [19], where D is the particle diameter, and λ the incident photon wavelength. This scattering process is respectively related to the size of the particle. For small scattering particles (see Fig. 4a), the distribution of scattered light is symmetric in the forward and backward directions. If the particle size increases, the scattered energy increases in the direction of the incident beam diminishing the amount of scattered light in the opposite direction [19] (see Fig. 4b, 4c).

The scattering cross-section Q_d [19] is proportional to the radiation-particle interaction probability, and it is defined through the so-called effective area of the collision. For which the total scattering of the impinging light is proportional to the effect cross-section (Mie theory [19]) multiplied by the amount of the particles present in the medium [19]. The scattering cross-section is here related to sp of the interacting particle through the probability of extinction of the photon, also known as the extinction efficiency, Q_{ext} [19], the scattering probability Q_{sca} [19], and the absorption probability Q_{abs} [19].

A. Fog effect in the spatial resolution

In scattering scenarios, present changes in the level of contrast in the scenes that affect the quality of the reconstructed 2D image, and deducting spatial resolution image. In the case of scenarios with fog the level contrast is defined by Beer–Lambert law [19], where the contrast decreases by an exponential factor with distance defined by Eq. (5), with β as scattering coefficients Eq. (6), and depend on Q_{sc} is the scattering coefficient (calculate using matlab [28]), the radius

of particles r and $D_{density}$ is the density of particles suspended in the medium.

$$C = C_o e^{-\beta z}. \tag{5}$$

$$\beta = D_{density} \pi r^2 Q_{ext} \tag{6}$$

Therefore, as the measurement distance increases, the SPC's ability for discriminate objects is reduced due to this scattering effect.

IV. THE MEASUREMENT OF SPATIAL RESOLUTION

A method to determine the spatial resolution is the point spread function (PSF) [12]. For the estimation of the PSF, we use a test object with known dimensions that consists an circle (use a geometric symmetric based on [11]) of a reflective material over a dark background [14]. This test image is reconstructed, and we calculate the PSF in the function of normalized contrast and dimensions of the test object. Considering the point where the value normalized of the contrast is 0.5, we can define the range spatial resolution through the full-width-at-half-maximum (FWHM) defined by Eq. (7) over PSF chart.

For obtaining the spatial resolution of the NIR-SPI image, first, determine the edge spread function (ESF), which is the result of the detection of edges changing over the image in binary that goes from 0 to 1. Then, with the ESF value, we can obtain the Line spread function (LSF) by the differentiation of ESF; using the LSF we can calculate the PSF. To calculate the PSF and obtain the spatial resolution, we define the following methodology:

1) Binary test image (test image circle [11], and lines see Figs. 8-10).
2) The shape of the edge is estimated by fitting to the edge pixels.
3) The ESF and LSF are estimated from the pixels in the vicinity of the edge. To this end, each pixel is characterized by two parameters:
   a) Intensity.
   b) NIR-SPI image displacement (negative for interior pixels, positive for the rest).
4) Orientation of the segment that connects the pixel with NIR-SPI image.
5) The calculation of the LSF to edge orientation is estimated by differentiating across the displacement dimension.
6) we applying FFT over LSF obtained the Modulation transfer function (MTF) parameter define of resolution contrast [8].
7) we applying 2D-FFT over the normalized MTF, and we can obtain the PSF over that we applied FWHM to calculate the spatial resolution σ, defined by Eq. (7)

$$FWHM = 2.36\sigma \tag{7}$$

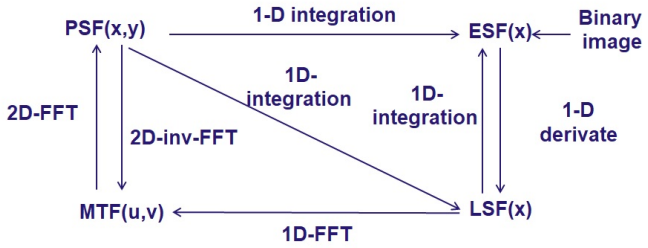

Fig. 5: Overview step to calculate the spatial resolution NIR-SPI imaging.

V. RESULTS

A. Experimental setup

To evaluate the NIR-SPI vision system's spatial resolution, we made two tests under the foggy without/with the condition: (i) we determinate as spatial resolution change with distance, for which using a shape symmetric (circle of 50 diameters) located range distance focal between 18 to 30 cm, in this test, we use the four scanning projection method (Basic, Hilbert, Zig-Zag, and Spiral), and 50 measurements were made for each of the projection methods, and (ii) we determinate the distance minimum separation between objects and the minimum width on-axis x and y, for which we use an array of lines. For evaluation, we developed a test bench that has a controlled system of illumination to simulate a light outdoor background with a range between 5 K to 50 KLux (we used a source light of the type semi-direct to simulate light outdoor background [3]) and a system that can simulate the conditions of fog size particles water with diameters of $@3\mu m$ that correspond a condition of heavy foggy of low visibility [3] (see Fig. 7). The chamber designed has dimensions of 60 × 40 × 25 cm, which an area test of 35 x 30 x 20 cm; the range of the maximum measurement is limited to 35 cm, and for the generation of artificial fog, we use a piezoelectric humidifier to operate in a frequency of 1.7 MHz, obtaining a water droplet of 3 μm Eq. (8) [3]. The droplet diameter as function of the piezoelectric frequency (see Fig. 6) Eq. (8), where σ_s surface tension (N/m), ρ density of the liquid (kg/m^3), f is the piezoelectric frequency.

$$d = 0.34 \left(\frac{8\pi\sigma_s}{\rho f^2} \right)^{1/3} \tag{8}$$

B. Discussion of result

In the test, we focus on determining the spatial resolution for a NIR-SPC under the foggy without/with the condition using the method defined in the section IV. In the first evaluation, located the test object ranging of distance from 18 to 30 cm, with that we can determine the spatial resolution in the function of the distance (see Fig. 9-8). In the short distance below 25 cm, the Spiral and Hilbert scanning have a spatial resolution of around 25 mm under foggy conditions and 20 mm without foggy conditions, and for the maximum

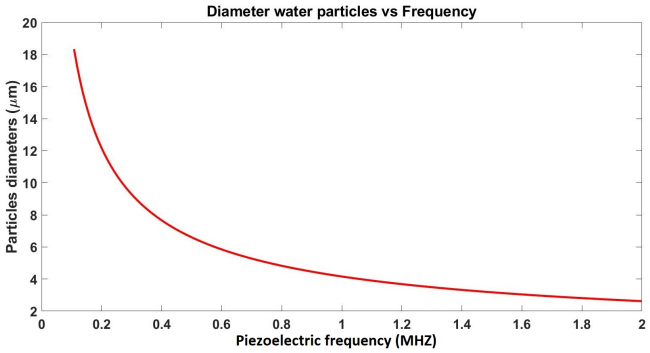

Fig. 6: The operating range (108.3 KHz to 1.7 MHz) of the used piezoelectric, in that range we can generate diameters particles fog between 3 μm to 180 μm.

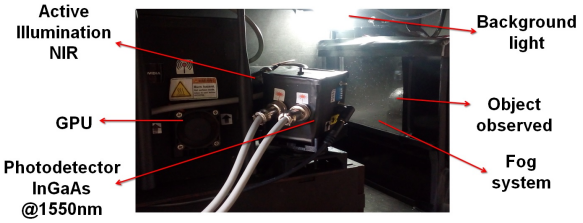

Fig. 7: Experimental setup for NIR-SPI vision system, the test bench has a control system for emulate fog and background condition, the test object should be placed in the glass box.

distance of 30 cm, the spatial resolution increase and reach values higher than 40 mm, limited the detection of small objects. In this condition, the Basic and Hilbert scanning methods have a better resolution below 50 mm under foggy conditions and 40 mm using Spiral under foggy conditions. With that, we have Hilbert scanning as the method with a better range of spatial resolution under foggy conditions and Spiral for without foggy conditions (see table II - III). In second test, using the Hilbert scanning method that present best spatial resolution, with that we determinate that minimum distance separation between object is 10 mm for both axis (see Fig. 10), and for simple shape the minimum width is

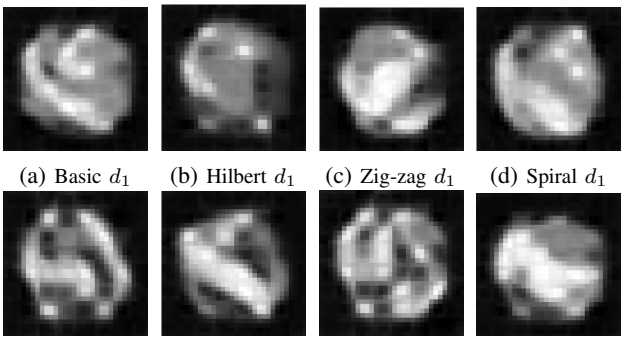

(a) Basic d_1 (b) Hilbert d_1 (c) Zig-zag d_1 (d) Spiral d_1

(e) Basic d_2 (f) Hilber d_2 (g) Zig-zag d_2 (h) Spiral d_2

Fig. 8: NIR-SPI test image circle of 50 diameter: At focal length distance d_1=18 cm, and d_2=30 cm , a-e) basic scanning, b-f) Hilbert scanning, c-g) Zig-Zag scanning, d-h) Spiral scanning.

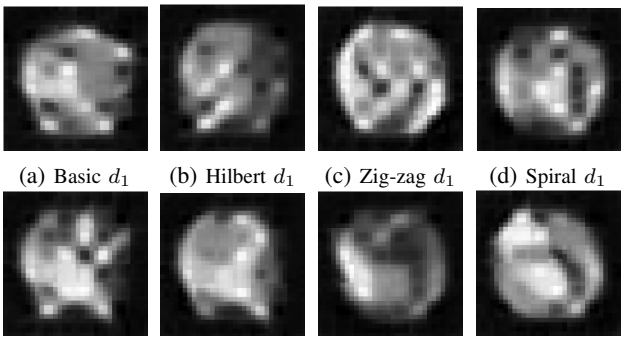

(a) Basic d_1 (b) Hilbert d_1 (c) Zig-zag d_1 (d) Spiral d_1

(e) Basic d_2 (f) Hilbert d_2 (g) Zig-zag d_2 (h) Spiral d_2

Fig. 9: NIR-SPI test image circle under foggy conditions of 50 diameter: At focal length distance d_1=18 cm, and d_2=30 cm, a-e) basic scanning, b-f) Hilbert scanning, c-g) Zig-Zag scanning, d-h) Spiral scanning.

TABLE II: Spatial resolution (mm) on scenario without fog using circle edge by distance:, d_1=18 cm, d_2=20 cm,d_3=25 cm, and d_4=30 cm.

Scanning method	$d_1(mm)$	$d_2(mm)$	$d_3(mm)$	$d_4(mm)$
Basic	12	14	18	23
Hilbert	8.72	12	19	23
Zig-Zag	10	16	30	39
Spiral	12.3	19	26.3	30

Δx=11.6 mm and Δy=12 mm without Fog (see Fig. 10a-10b), and Δx=16 mm and Δy=18 mm with Fog (see Fig. 10c-10d).

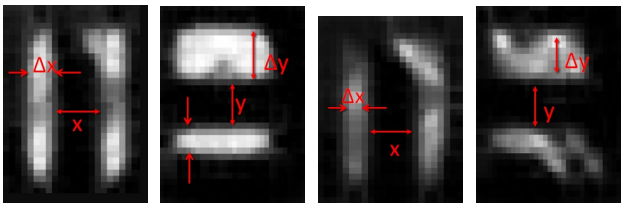

(a) (b) (c) (d)

Fig. 10: Spatial resolution using Hilbert Scanning at 20 cm , with separation between x=10 mm and y=10 mm Δx=11.6 mm and Δy=12 mm without Fog (a-b), and Δx=16 mm and Δy=18 mm with Fog (c-d).

VI. CONCLUSION

This paper analyzes the spatial resolution of an SPC system that works in the near-infrared (NIR) under foggy and without foggy conditions. From the SPI image, we determine the spatial resolution by applying the method of MTF by using

TABLE III: Spatial resolution (mm) on scenario with fog using circle edge by distance: d_1=18 cm, d_2=20 cm,d_3=25 cm, and d_4=30 cm.

Scanning method	d_1(mm)	d_2(mm)	d_3(mm)	d_4(mm)
Basic	16	19.3	26	38
Hilbert	12	16	30	40
Zig-Zag	15	21	35	47
Spiral	16	22	31	35

TABLE IV: Change of the eccentric of the test image circle under foggy without/with condition by distance: d_1=18 cm,and d_2=30 cm.

Scanning method	e_{d1not_fog}	e_{d2not_fog}	e_{d1_fog}	e_{d2_fog}
Basic	0.75	0.69	0.73	0.6
Hilbert	0.76	0.7	0.71	0.52
Zig-Zag	0.79	0.71	0.71	0.63
Spiral	0.88	0.8	0.75	0.65

a slanted edge target [14]. To evaluate the spatial resolution range, we made two testings. In the first, we determine that in the short distance below 25 cm, if we use Spiral or Hilbert scanning, we can get a small detection object with a resolution of 20 mm under foggy conditions and below 20 mm scenarios without fog, and the maximum distance of 30 cm the spatial resolution is higher than 40 mm. For shape symmetric, we see that Zig-Zag and Spiral scanning present less loss in the edge information to far distance, and under foggy condition, Spiral have the best spatial resolution (see Table IV).

REFERENCES

[1] C. A. Osorio Quero, D. Durini, J. Rangel-Magdaleno, and J. Martinez-Carranza, "Single-pixel imaging: An overview of different methods to be used for 3d space reconstruction in harsh environments," *Review of Scientific Instruments*, vol. 92, no. 11, p. 111501, 2021. [Online]. Available: https://doi.org/10.1063/5.0050358

[2] C. O. Quero, D. Durini, R. Ramos-Garcia, J. Rangel-Magdaleno, and J. Martinez-Carranza, "Hardware parallel architecture proposed to accelerate the orthogonal matching pursuit compressive sensing reconstruction," in *Computational Imaging V*, L. Tian, J. C. Petruccelli, and C. Preza, Eds., vol. 11396, International Society for Optics and Photonics. SPIE, 2020, pp. 56 – 63. [Online]. Available: https://doi.org/10.1117/12.2558937

[3] C. O. Quero, D. D. Romero, J. Rangel-Magdaleno, J. Martinez-Carranza, and R. Ramos-Garcia, "2D/3D single-pixel NIR image reconstruction method for outdoor applications in presence of rain," in *SPIE Future Sensing Technologies 2021*, M. Kimata, J. A. Shaw, and C. R. Valenta, Eds., vol. 11914, International Society for Optics and Photonics. SPIE, 2021, pp. 224 – 243. [Online]. Available: https://doi.org/10.1117/12.2601118

[4] D. Shrekenhamer, C. M. Watts, and W. J. Padilla, "Terahertz single pixel imaging with an optically controlled dynamic spatial light modulator," *Opt. Express*, vol. 21, no. 10, pp. 12 507–12 518, May 2013. [Online]. Available: http://www.osapublishing.org/oe/abstract.cfm?URI=oe-21-10-12507

[5] J. Ma, "Single-pixel remote sensing," *IEEE Geoscience and Remote Sensing Letters*, vol. 6, no. 2, pp. 199–203, 2009.

[6] C. Leung and T. D. Donnelly, "Measuring the spatial resolution of an optical system in an undergraduate optics laboratory," *American Journal of Physics*, vol. 85, no. 6, pp. 429–438, 2017. [Online]. Available: https://doi.org/10.1119/1.4979539

[7] L.-C. Liu, L.-Y. Qu, C. Wu, J. Cotler, F. Ma, M.-Y. Zheng, X.-P. Xie, Y.-A. Chen, Q. Zhang, F. Wilczek, and J.-W. Pan, "Improved spatial resolution achieved by chromatic intensity interferometry," *Phys. Rev. Lett.*, vol. 127, p. 103601, Aug 2021. [Online]. Available: https://link.aps.org/doi/10.1103/PhysRevLett.127.103601

[8] G. Boreman, "Mtf in optical systems," in *Modulation Transfer Function in Optical and Electro-Optical Systems*. SPIE, 2001, pp. 1–30.

[9] F. Viallefont-Robinet, D. Helder, R. Fraisse, A. Newbury, F. van den Bergh, D. Lee, and S. Saunier, "Comparison of mtf measurements using edge method: towards reference data set," *Opt. Express*, vol. 26, no. 26, pp. 33 625–33 648, Dec 2018. [Online]. Available: http://opg.optica.org/oe/abstract.cfm?URI=oe-26-26-33625

[10] C. Damian and D. Coltuc, "Measurement of non-circular psfs in single pixel cameras," in *2018 International Conference on Communications (COMM)*, 2018, pp. 1–124.

[11] C. Damian, F. Garoi, C. Udrea, and D. Coltuc, "The evaluation of single-pixel camera resolution," *IEEE Transactions on Circuits and Systems for Video Technology*, vol. 30, no. 8, pp. 2517–2523, 2020.

[12] D. N. R. Payne, M. K. Juhl, M. E. Pollard, A. Teal, and D. M. Bagnall, "Evaluating the accuracy of point spread function deconvolutions applied to luminescence images," in *2016 IEEE 43rd Photovoltaic Specialists Conference (PVSC)*, 2016, pp. 1585–1589.

[13] K. Fliegel, "Modeling and measurement of image sensor characteristics," *Radioengineering*, vol. 13, 12 2004.

[14] B. Theron, M. El-Desouki, F. M. R. Aljekhedab, M. S. I. Alayed, and M. S. D. Alsawadi, "Choice of spatial resolution measurement methods to implement," in *2013 Saudi International Electronics, Communications and Photonics Conference*, 2013, pp. 1–5.

[15] R. L. Baer, "Circular-edge spatial frequency response test," in *Image Quality and System Performance*, Y. Miyake and D. R. Rasmussen, Eds., vol. 5294, International Society for Optics and Photonics. SPIE, 2003, pp. 71 – 81. [Online]. Available: https://doi.org/10.1117/12.524829

[16] K. Masaoka, "Accuracy and precision of edge-based modulation transfer function measurement for sampled imaging systems," *IEEE Access*, vol. 6, pp. 41 079–41 086, 2018.

[17] V. Twersky, "Rayleigh scattering," *Appl. Opt.*, vol. 3, no. 10, pp. 1150–1162, Oct 1964. [Online]. Available: http://opg.optica.org/ao/abstract.cfm?URI=ao-3-10-1150

[18] B. Theron, M. El-Desouki, F. M. R. Aljekhedab, M. S. I. Alayed, and M. S. D. Alsawadi, "Choice of spatial resolution measurement methods to implement," in *2013 Saudi International Electronics, Communications and Photonics Conference*, 2013, pp. 1–5.

[19] C. Osorio Quero, D. Durini, J. Rangel-Magdaleno, J. Martinez-Carranza, and R. Ramos-Garcia, "Single-pixel near-infrared 3d image reconstruction in outdoor conditions," *Micromachines*, vol. 13, no. 5, 2022. [Online]. Available: https://www.mdpi.com/2072-666X/13/5/795

[20] G. M. Gibson, S. D. Johnson, and M. J. Padgett, "Single-pixel imaging 12 years on: a review," *Opt. Express*, vol. 28, no. 19, pp. 28 190–28 208, Sep 2020. [Online]. Available: http://www.opticsexpress.org/abstract.cfm?URI=oe-28-19-28190

[21] Z. Zhang, X. Wang, G. Zheng, and J. Zhong, "Hadamard single-pixel imaging versus fourier single-pixel imaging," *Opt. Express*, vol. 25, no. 16, pp. 19 619–19 639, Aug 2017. [Online]. Available: http://www.opticsexpress.org/abstract.cfm?URI=oe-25-16-19619

[22] H. Ma, A. Sang, C. Zhou, X. An, and L. Song, "A zigzag scanning ordering of four-dimensional walsh basis for single-pixel imaging," *Optics Communications*, vol. 443, pp. 69–75, 2019. [Online]. Available: https://www.sciencedirect.com/science/article/pii/S0030401819301506

[23] T. M. Cabreira, C. D. Franco, P. R. Ferreira, and G. C. Buttazzo, "Energy-aware spiral coverage path planning for uav photogrammetric applications," *IEEE Robotics and Automation Letters*, vol. 3, no. 4, pp. 3662–3668, 2018.

[24] U. Ujang, F. Anton, S. Azri, A. Rahman, and D. Mioc, "3d hilbert space filling curves in 3d city modeling for faster spatial queries," *International Journal of 3D Information Modeling (IJ3DIM)*, 04 2014.

[25] R. Lange, S. Böhmer, and B. Buxbaum, "11 - cmos-based optical time-of-flight 3d imaging and ranging," in *High Performance Silicon Imaging (Second Edition)*, second edition ed., ser. Woodhead Publishing Series in Electronic and Optical Materials, D. Durini, Ed. Woodhead Publishing, 2020, pp. 319–375. [Online]. Available: https://www.sciencedirect.com/science/article/pii/B9780081024348000118

[26] C. A. Osorio Quero, D. D. Romero, R. Ramos-Garcia, J. de Jesus Rangel-Magdaleno, and J. Martinez-Carranza, "Towards a 3d vision system based on single-pixel imaging and indirect time-of-flight for drone applications," in *2020 17th International Conference on Electrical Engineering, Computing Science and Automatic Control (CCE)*, 2020, pp. 1–6.

[27] K.-N. Liou, "An introduction to atmospheric radiation / kuo-nan liou." New York, 1980.

[28] C. Matzler, "Matlab functions for mie scattering and absorption," *IAP Res Rep*, vol. 8, 07 2002.